CHEMISTRY
A EUROPEAN JOURNAL

FULL PAPER

DOI: 10.1002/chem.201202072

IR-Monitored Photolysis of CO-Inhibited Nitrogenase: A Major EPR-Silent Species with Coupled Terminal CO Ligands

Lifen Yan,[a] Vladimir Pelmenschikov,*[b] Christie H. Dapper,[c] Aubrey D. Scott,[a] William E. Newton,[c] and Stephen P. Cramer*[a, d]

Abstract: Fourier transform infrared spectroscopy (FTIR) was used to observe the photolysis and recombination of a new EPR-silent CO-inhibited form of α-H195Q nitrogenase from *Azotobacter vinelandii*. Photolysis at 4 K reveals a strong negative IR difference band at $\tilde{\nu}=1938\,cm^{-1}$, along with a weaker negative feature at $1911\,cm^{-1}$. These bands and the associated chemical species have both been assigned the label "Hi-3". A positive band at $\tilde{\nu}=1921\,cm^{-1}$ was assigned to the "Lo-3" photoproduct. By using an isotopic mixture of $^{12}C^{16}O$ and $^{13}C^{18}O$, we show that the Hi-3 bands arise from coupling of two similar CO oscillators with one uncoupled frequency at approximately $\tilde{\nu}=1917\,cm^{-1}$. Although in previous studies Lo-3 was not observed to recombine, by extending the observation range to 200–240 K, we found that recombination to Hi-3 does indeed occur, with an activation energy of approximately $6.5\,kJ\,mol^{-1}$. The frequencies of the Hi-3 bands suggest terminal CO ligation. This hypothesis was tested with DFT calculations on models with terminal CO ligands on Fe2 and Fe6 of the FeMo-cofactor. An $S=0$ model with both CO ligands in *exo* positions predicts symmetric and asymmetric stretches at $\tilde{\nu}=1938$ and $1909\,cm^{-1}$, respectively, with relative band intensities of about 3.5:1, which is in good agreement with experiment. From the observed IR intensities, Hi-3 was found to be present at a concentration about equal to that of the EPR-active Hi-1 species. The relevance of Hi-3 to the nitrogenase catalytic mechanism and its recently discovered Fischer–Tropsch chemistry is discussed.

Keywords: density functional calculations · IR spectroscopy · Fischer–Tropsch · nitrogenase · photolysis

Introduction

The enzymatic nitrogen fixation system known as nitrogenase (N_2ase) catalyzes the reduction of dinitrogen to ammonia at ambient temperatures and atmospheric pressure.[1] For the Mo-dependent N_2ase, binding of substrates and inhibitors involves a [Mo-7Fe-9S-**X**]-homocitrate-containing prosthetic group, called the FeMo-cofactor, of the larger MoFe protein (*Av1*). A recent crystal structure at 1.0 Å resolution[2] and an X-ray emission study[3] favor assigning C^{4-} carbide as the much-debated atom **X** at the center of the cofactor. The mechanism, by which this biological nanoparticle lowers the activation energy for reduction of the N≡N triple bond, remains incompletely understood.

Carbon monoxide inhibits the reduction of N_2 reversibly and noncompetitively, and CO has been an important probe molecule for characterizing the active site.[4] Recently, Ribbe and co-workers have shown that CO can actually be a substrate for the V version of N_2ase,[5] and with less efficiency, even for the wild-type Mo-dependent N_2ase.[6] Seefeldt and co-workers have also demonstrated CO fixation by using the α-V70A and other variants of the MoFe protein.[7] Thus, a second front of interest in N_2ase as a Fischer–Tropsch catalyst has emerged.[8]

Exposure of N_2ase to CO during turnover elicits species with a variety of EPR signals, depending on the partial pressure of CO ([CO]), and each of these species and its characteristic EPR signal is described by the [CO] required for its formation.[9] The chemical species and its associated axial EPR signal (g values ~2.17 and ~2.06) are both called hi-CO and are formed under approximately 101 kPa [CO]. This hi-CO N_2ase species is proposed to contain two CO molecules bound to the FeMo-cofactor.[9–10] A species with a rhombic EPR spectrum (g values of 2.09, 1.98, and 1.93) called lo-CO forms under a much lower [CO][11] and is proposed to contain only one bound CO.[9–10] A third species

[a] L. Yan, A. D. Scott, Prof. S. P. Cramer
Department of Chemistry
University of California, Davis, CA 95616 (USA)
E-mail: spjcramer@ucdavis.edu

[b] Dr. V. Pelmenschikov
Institut für Chemie
Technische Universität Berlin
10623 Berlin (Germany)
E-mail: pelmentschikov@mailbox.tu-berlin.de

[c] C. H. Dapper, Prof. W. E. Newton
Department of Biochemistry
Virginia Polytechnic Institute and State University
Blacksburg, VA 24061 (USA)

[d] Prof. S. P. Cramer
Physical Biosciences Division
Lawrence Berkeley National Laboratory
Berkeley, CA 94720 (USA)
E-mail: spcramer@lbl.gov

Supporting information for this article is available on the WWW under http://dx.doi.org/10.1002/chem.201202072.

and EPR signal, both called hi(5)-CO, have also been identified.[11c,d] Not all of these EPR signals are generated when variant Mo N_2ases are turned over under CO,[12] and the integrated EPR intensities rarely exceed 40% of the active-site species.[11d] Presumably, EPR-silent species with bound CO must co-exist with the EPR-active species.

Another spectroscopic tool that complements EPR for these studies has been FTIR spectroscopy.[4c,13] In stopped-flow FTIR experiments, under low [CO], a single $\tilde{\nu}$(CO) band appeared at 1904 cm^{-1} and peaked in intensity within approximately 7 s before decaying. Under high [CO], a new $\tilde{\nu}$(CO) band was observed at 1936 cm^{-1} together with a pair of weaker, possibly coupled bands at $\tilde{\nu}$ = 1958 and 1880 cm^{-1}. All of these features were much longer lived than the 1904 cm^{-1} band. All three species were suggested to arise from terminally bound CO. After relatively long times (>10 s), under low [CO] the 1904 cm^{-1} peak is succeeded by a new $\tilde{\nu}$(CO) band at 1715 cm^{-1}. Recently, the rates and relative intensities of these $\tilde{\nu}$(CO) bands were shown to be sensitive to variation of the side chain at the α-70 position.[13c] Other CO-related IR bands have been observed during spectroelectrochemical studies of FeMoco (the solvent-extracted version of the FeMo-cofactor),[14] in which bands at $\tilde{\nu}$ = 1808 and 1835 cm^{-1} were proposed to arise from bridging CO, whereas features at $\tilde{\nu}$ = 1885 and 1920 cm^{-1} were assigned to terminally bound CO species.

In a recent study of CO-inhibited *Azotobacter vinelandii* Mo nitrogenase, we showed that FTIR can be used to monitor CO photolysis by visible light at cryogenic temperatures.[15] Three distinct types of photolyzable CO complexes were found under hi-CO conditions. We labeled these stable inhibited forms "Hi-1", "Hi-2", and "Hi-3". The photolyses of Hi-1 and Hi-2 were found to be reversible at around 80 K, with activation energies on the order of 3–4 kJ mol^{-1}. However, the Hi-3 photoproduct, labeled "Lo-3", was stable with respect to recombination up to 110 K. The Hi-3 species was most abundant in the photolysis spectra of N_2ase with the variant α-H195Q MoFe protein. Herein, we have used this variant and an extended temperature range (ca. 200–250 K) to discover that Hi-3 photolysis is also reversible. Mixed CO isotopes were used to demonstrate vibrational coupling in the Hi-3 species, and wavelength-dependent photolysis—to determine the spectral region with the greatest photochemical activity. The relative amounts of the Hi-1 and Hi-3 species in our samples were also estimated. Finally, DFT calculations were employed to evaluate plausible structures for Hi-3 and Lo-3 CO-bound FeMo-cofactor species.

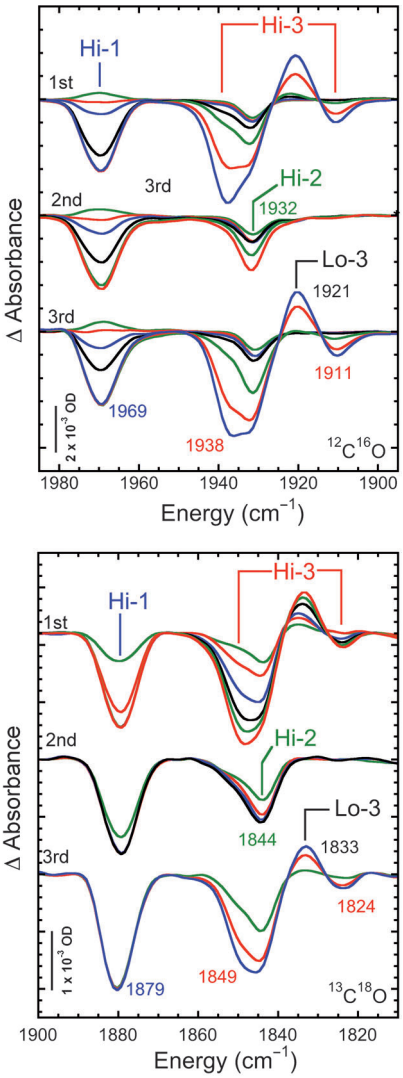

Figure 1. Time-dependent absorbance changes upon photolysis at 4 K and thermal cycling of CO-inhibited α-H195Q nitrogenase in D_2O-based HEPES buffer (25 mM, pH 7.4) with ethylene glycol (40%). Top: "hi-$^{12}C^{16}O$" conditions; top to bottom: 1st photolysis, time points shown: 0.5, 4, 9, 52 s, 3, 30, and 150 min; 2nd photolysis, after warming to 120 K for 20 min, time points shown: 0.5, 7, 13, 35 s, 2, and 30 min; 3rd photolysis after poising at approximately 263 K for 16 h, time points shown: 0.5, 5, 13, 30 s, 5, 70, and 270 min. Bottom: "hi-$^{13}C^{18}O$" conditions; top to bottom: 1st photolysis, time points shown: 0.5, 2, 10, 31, 60, and 122 min; 2nd photolysis, after warming sample to 120 K for 10 min, time points shown: 2, 10, 30, and 60 min; 3rd photolysis, after warming sample to 233 K for 8 h, time points shown: 3, 23, and 63 min.

Results

Photolysis: Figure 1 shows the time courses of changes in the IR spectra of CO-inhibited α-H195Q N_2ase samples illuminated with visible light at approximately 4 K under either $^{12}C^{16}O$ or $^{13}C^{18}O$. Photolysis spectra under $^{13}C^{16}O$ are included in Figure 2. At long times, the largest spectral changes come from the Hi-3 species,[15] with a strong negative band at $\tilde{\nu}$ = 1938 cm^{-1} (1894, 1849) and a weaker negative band at 1911 cm^{-1} (1867, 1824). A positive product band from Lo-3 is seen in between these two bands at $\tilde{\nu}$ = 1921 cm^{-1} (1877, 1833; in these and later descriptions, the first value refers to results with $^{12}C^{16}O$, whereas the second and third values in parentheses, if present, refer to results with $^{13}C^{16}O$ and $^{13}C^{18}O$, respectively.) As was noted before,[15] for α-H195Q N_2ase, the spectra are complicated by the presence of other photolyzable species, including

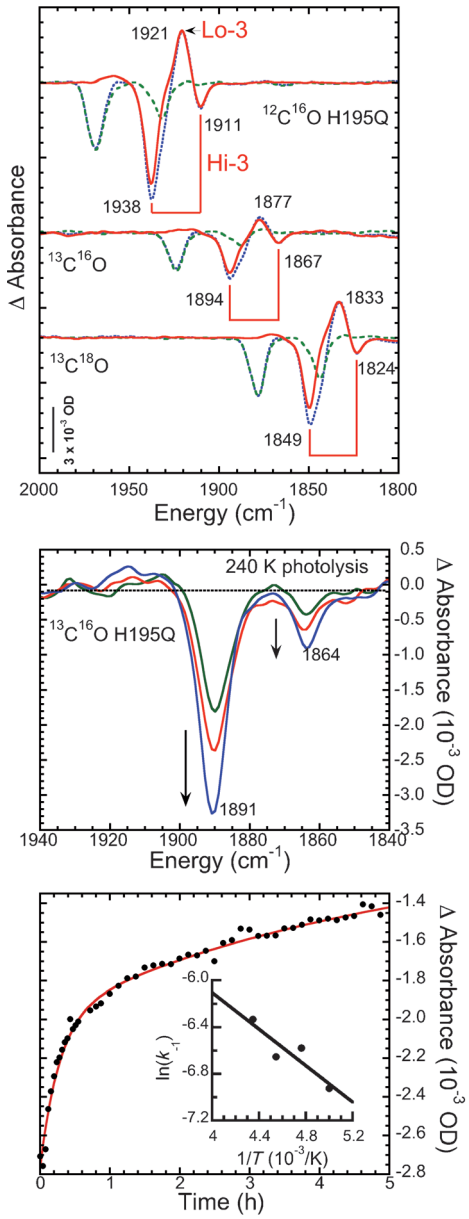

Figure 2. Top: extraction of Hi-3/Lo-3 spectra (red ——) by subtraction of 2nd photolysis spectra (green – – –; photolyzed at 4 K after recombination at 120 K) from 1st spectra (blue – – –). Middle: photolysis at 240 K. Times are 40 (green ——), 60 (red ——), and 150 min (black ——). Bottom: recombination data for 210 K, fit with dual exponential. Inset: Arrhenius plot for fast phase of recombination, yielding an activation energy of 6.5 kJ mol^{-1}.

bands for Hi-1 at $\tilde{\nu}=1969$ (1925, 1879) and for Hi-2 at 1932 cm^{-1} (1888, 1844).

The spectra can be simplified by employing the fact that the photolysis product Lo-3 is relatively stable at temperatures, in which the photolysis products from Hi-1 and Hi-2 rapidly recombine.[15] Accordingly, the photolyzed samples were warmed to 120 K for 10–20 min and then photolyzed a second time. As shown in Figure 1, there was almost no trace of the Hi-3 or Lo-3 features in the second photolysis spectrum, which is consistent with the absence of Hi-3. By taking the difference between the two photolysis results, a relatively pure Hi-3→Lo-3 photolysis signal was obtained in the double-difference spectrum (Figure 2). The extracted spectrum exhibited almost pure Hi-3 features at the same frequencies as was noted in the mixed spectra. Note that in the third photolysis spectrum, which followed warming the sample from the second photolysis to above 230 K, the Hi-3→Lo-3 signals reappeared.

An alternative method of cleanly separating the Hi-3 features is to photolyze at higher temperatures, in which the recombination of the other photolysis products is fast. As shown in Figure 2, photolysis of a $^{13}C^{16}O$ sample at 240 K gave a spectrum with a pair of negative bands at $\tilde{\nu}=1891$ and 1864 cm^{-1}; nearly the same as the frequencies (1894 and 1867 cm^{-1}) seen in the low-temperature photolysis. In fact, the 3 cm^{-1} downshifts are similar to those seen in myoglobin–CO upon raising the temperature from 4 K to room temperature.[16] This observation suggests that comparable shifts between our liquid-helium-temperature photolysis results and the room-temperature stopped-flow FTIR studies should be anticipated. In these higher temperature photolyses, there was less evidence of the Lo-3 photolysis product. We cannot exclude the possibility that additional processes involving CO migration and rearrangement and/or possible Lo-3 photolysis might be occurring at higher temperatures; these issues call for additional study.

Recombination: As can be seen from Figure 2, Hi-3 returns on the 1 h time scale upon warming the sample to approximately 210 K. From monitoring this process at various temperatures, Arrhenius plot analysis by using the initial rates gave an activation energy of about 6.5 kJ mol^{-1} (Figure 2), compared to the approximately 4 kJ mol^{-1} values previously seen for Hi-1 and Hi-2 recombination.[15] (In more recent studies, we have found that with brief irradiation, the Hi-2 recombination can occur with a much smaller activation energy).[17] The Hi-3 value is similar to the barriers of 8–10 kJ mol^{-1} seen for Ni-SI$_a$→NiSCO CO recombination in [NiFe] hydrogenases[18] and for photolyzed MbCO.[19]

Mixed isotope studies: The relative intensities of the negative Hi-3→Lo-3 features involve a higher 1938 cm^{-1} (1894, 1849) frequency band that is about four times stronger than its lower 1911 cm^{-1} (1867, 1824) frequency partner. One explanation for the different intensities of the high and low frequency bands is that they represent the symmetric (with I_{sym} intensity) and antisymmetric (I_{asym}) combinations of stretches for two distinct terminally bound CO molecules. Assuming that the symmetric combination has the higher frequency, the equation $I_{sym}/I_{asym}=\cot^2\theta$, in which θ is half the angle between the CO molecular axes, can be used to calculate a rough approximation of the relative orientations of the two molecules.[20] For an intensity ratio of about four, the angle 2θ between CO axes is predicted to be approximately 50°. Such an angle is too small for two CO molecules bound at the same metal ion. Furthermore, coupling of vicinal $^{12}C^{16}O$ molecules usually produces splitting of about 40–

60 cm^{-1},[20] approximately twice as large as that observed for Hi-3. Both observations support the notion that there are two vibrationally coupled CO ligands, each of which is bound to a different FeMo-cofactor metal ion.

To confirm the assignment of the Hi-3 signals to coupled oscillators, photolysis spectra for α-H195Q N_2ase inhibited by a mixture of approximately 25% $^{12}C^{16}O$ and approximately 75% $^{13}C^{18}O$ were recorded. In the absence of coupling, such a sample would produce a spectrum that is the 25:75 = 1:3 weighted average of the two pure 100% $^{12}C^{16}O$ and 100% $^{13}C^{18}O$ spectra, respectively. However, as can be seen from Figure 3, the mixed-CO spectrum has a new negative band at $\tilde{\nu}$ = 1917 cm^{-1}. This band does not appear in the second photolysis spectrum after recombination at 120 K (see Figure 1), so we can rule out assigning it to either Hi-1 or Hi-2. As was expected for a Hi-3 assignment, the 1917 cm^{-1} band does reappear in the third-time photolysis, after recombination overnight at 233 K. We interpret this new band as resulting from photolysis of a Hi-3 species involving uncoupled CO oscillators, one with $^{12}C^{16}O$ and the other with $^{13}C^{18}O$. Thus, at least one of the CO ligands is predicted to have an uncoupled frequency of $\tilde{\nu}$ = 1917 cm^{-1}.

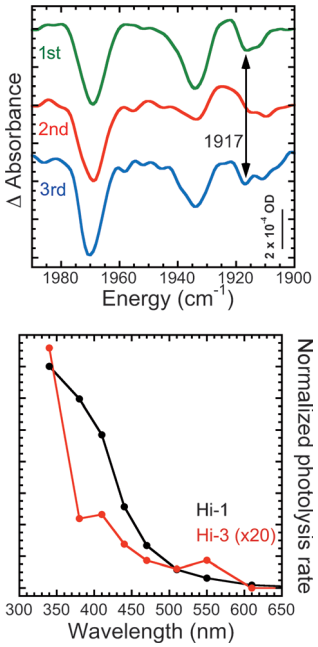

Figure 3. Top: mixed isotope effects on CO-inhibited nitrogenase. Top to bottom: 1st photolysis for 122 min; 2nd photolysis for 60 min, after warming to 120 K for 10 min; 3rd photolysis for 63 min, after warming to 233 K for 8 h. Bottom: wavelength dependence of Hi-3 photolysis versus Hi-1 photolysis.

Wavelength-dependent photolysis: To date, we have identified three forms of CO-inhibited N_2ase that are produced under high [CO] conditions and are photolyzed by exposure to white light. To better distinguish these species, the wavelength dependence of the photolysis rates was investigated, and the results of these studies are shown in Figure 3. The Hi-3 photolysis rate rises from near zero at λ = 600 to maximum efficiency at 340 nm, the shortest wavelength investigated. There appear to be minor features at about 550 and 400 nm. By comparison, the Hi-1 species, which we associate with the hi-CO EPR species previously examined by Maskos and Hales, exhibits a structureless rise in photolysis efficiency towards shorter wavelengths.[21] For Hi-1, we did not see the minor peak in the photolysis yield at about ~550 nm that was observed in the previous EPR experiments.[21]

DFT calculations: To put speculation about the structure of the Hi-3 species on firmer ground, DFT calculations were used to investigate models that involve pairs of terminal CO ligands on different FeMo-cofactor metal sites. With eight metal ions, there are 8(8−1)/2 = 28 possible pairs of binding sites on this prosthetic group. For the current study, the calculations were limited to binding at the most commonly proposed sites, the Fe2 and Fe6 ions on the face adjacent to the α-V70 residue (Figure 4).[13c,22] The atom and residue numbering herein are similar to the crystal structure.[23] As was described in a recent study by Dance,[24] we considered *exo* (CO *trans* to the central **X** atom, now known to be carbon) and *endo* (CO *trans* to μ^3 sulfurs, S1A/S1B when coordinated at Fe2/Fe6, respectively) terminal binding modes, which are subsequently referred as "Fe2/Fe6 *exo*/*endo*". A less popular bridging binding mode,[25] in which the CO carbon occupies a position similar to that of μ^2 S2B sulfur, was also considered. Below, we will discuss mostly those CO coordination modes that were found to be relevant in context of the Hi-3 and Lo-3 photolytic species; a detailed description of the binding alternatives will be covered separately.

Our favored model for Hi-3 is shown in Figure 4. In the DFT calculation, we assumed an S = 0 EPR-silent state for the FeMo-cofactor, $1e^-$ reduced from the S = 3/2 resting state. Other details on the metal-oxidation states and spin coupling are given in the Supporting Information. In line with earlier modeling by us and many others,[26] the central ligand **X** was initially assigned as N^{3-}. Subsequently, as described below, we considered the **X**=C^{4-} alternative, which has recently received significant support.[2–3,27] The μ^2 S2B sulfur that bridges Fe2 and Fe6 and forms the hydrogen bond to α-H195 in the wild-type enzyme was chosen as the protonation site for all the models. Terminal CO ligands are at Fe2 and Fe6, both in the *exo* geometry, and the Fe−C≡O bond angles are essentially 180° (Figure 4). This model predicts two coupled $^{12}C^{16}O$ stretching modes, a symmetric stretch at $\tilde{\nu}$ = 1938 and an asymmetric stretch at 1909 cm^{-1}, with relative band intensities of about 3.5:1, which is in good agreement with the experimental frequencies of $\tilde{\nu}$ = 1938 and 1911 cm^{-1} and amplitude ratio of about 3.7:1. (Here and below, the broadened peak-center heights are compared relative to the FTIR, see Figure 5, in contrast to the raw "stick" DFT mode intensities in Table S2 in the Supporting Information.) The optimized angle between the bound CO molecular axes is 37°, which is in line with the

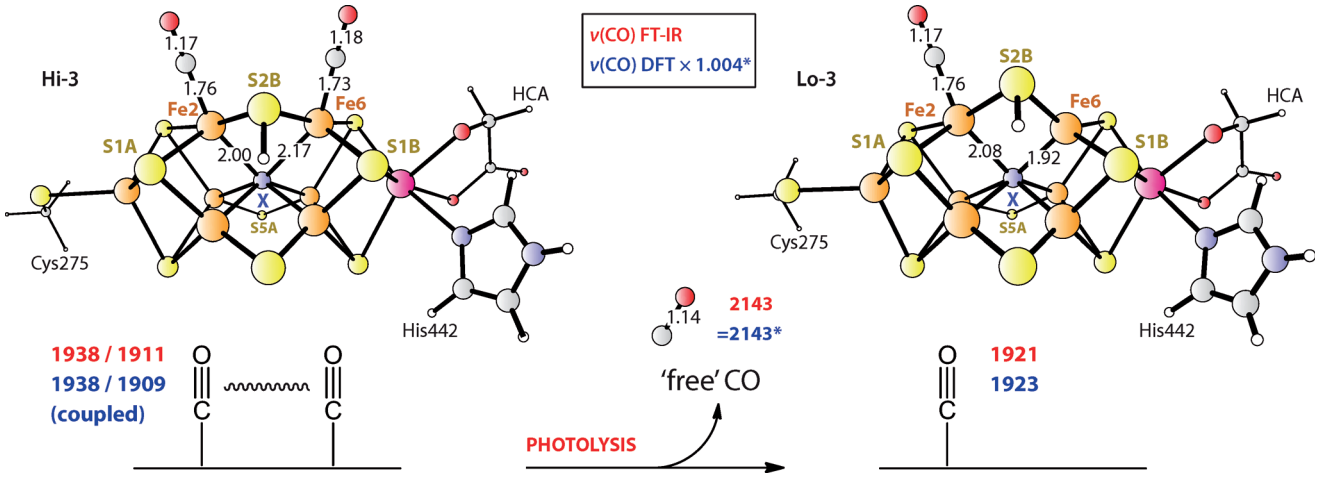

Figure 4. Favored DFT-optimized Hi-3 and Lo-3 structures. The observed FTIR (red) and calculated DFT (blue) frequencies [cm^{-1}] are given for the **X**=N^{3-} models. Selected interatomic distances [Å] are shown. Similar results were obtained with the now-favored **X**=C^{4-} assignment, provided μ^2 S5A sulfur was also protonated (see text). The asterisk implies DFT frequency scaling as described in the Supporting Information. For the model coordinates and animated vibrational modes, see the Supporting Information.

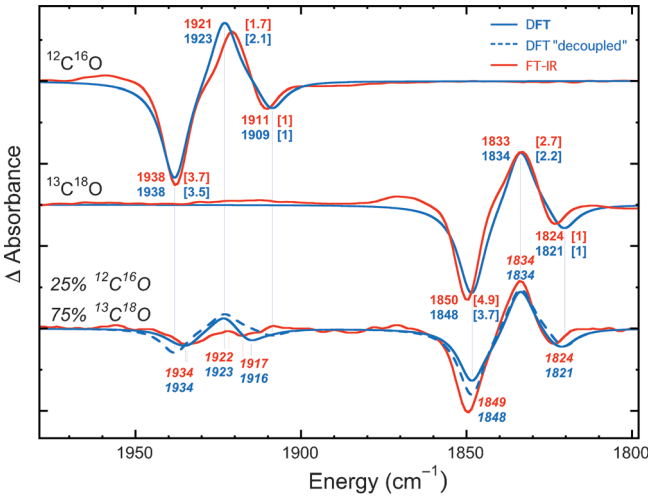

Figure 5. Overlay of the FTIR (red) versus DFT modeling (blue) of the Hi-3→Lo-3 photolysis difference spectra for pure $^{12}C^{16}O$ (top) and $^{13}C^{18}O$ (middle), and the mixed 25% $^{12}C^{16}O$/75% $^{13}C^{18}O$ (bottom) isotope experiments. The observed FTIR and calculated DFT frequencies are in cm^{-1}; the wave numbers for the mixed isotope case are in italic for clarity. For the pure isotope spectra, the peak intensities are given in square brackets relatively to the lower frequency Hi-3 band. The simulation of the hypothetical "decoupled" mixed isotope spectrum is presented as the broken line; the vertical lines imply that this spectrum provides no peak shifts with respect to the pure isotope spectra.

above 50° rough estimate based on the relative FTIR Hi-3 intensities. The basic FeMo-cofactor framework remained intact. However, a significant lengthening of the Fe6–**X** bond to 2.17 Å, compared with an average of 2.00 Å for the remaining optimized central Fe–**X** distances was noted. The plasticity of the FeMo-cofactor core has been observed in other calculations, in which even a complete loss of Fe coordination to **X** (Fe–**X** >3.0 Å) upon ligand binding has been predicted.[24,26c]

For the Lo-3 photolysis product, the structure with the best match to the FTIR Lo-3 band at $\tilde{\nu}=1921\ cm^{-1}$ involved Fe2 *exo* binding, producing a $^{12}C^{16}O$ frequency at $\tilde{\nu}=1923\ cm^{-1}$ (Figure 4). The calculated band intensity of this $\tilde{\nu}$(CO) stretch is about 2.1:1 relative to the asymmetric Hi-3 mode at $\tilde{\nu}=1909\ cm^{-1}$, in reasonable agreement with the approximately 1.7:1 ratio observed in the experiment. For photolysis conducted using the pure $^{13}C^{18}O$ isotope, the DFT results are essentially of the same quality as those described above for $^{12}C^{16}O$.

The calculations also shed light on our mixed isotope experiments. For models with $^{12}C^{16}O$ at Fe2 *exo* or Fe6 *exo* positions (and the other Fe site populated by $^{13}C^{18}O$), they predicted essentially "uncoupled" pairs of $\tilde{\nu}$(CO) frequencies of 1934/1825 or 1916/1842 cm^{-1}, respectively (for the animated vibrational modes, see the Supporting Information). We also modeled the actual Hi-3→Lo-3 photolysis IR spectra for 100% $^{12}C^{16}O$, 100% $^{13}C^{18}O$, and mixed isotope of 25% $^{12}C^{16}O$/75% $^{13}C^{18}O$ experiments by using our DFT frequency and intensity predictions (for details, see Table S1 in the Supporting Information). Figure 5 shows that in the low-frequency region, $\tilde{\nu}=1810$–$1860\ cm^{-1}$, the mixed isotope spectrum is dominated by the $^{13}C^{18}O$/$^{13}C^{18}O$ contributions, and the decoupled $^{13}C^{18}O$ bands are obscured by these features. However, in the higher-frequency region, $\tilde{\nu}=1900$–$1950\ cm^{-1}$, the mixed isotope species provides most of the intensity, and the DFT peaks at $\tilde{\nu}=1934$ and $1916\ cm^{-1}$ show noticeable shifts (of −4 and +7 cm^{-1}) with respect to the pure $^{12}C^{16}O$ isotope Hi-3 features. The FTIR bands seen at $\tilde{\nu}=1934$ and $1917\ cm^{-1}$ can now be assigned to essentially uncoupled stretching modes of the $^{12}C^{16}O$ at Fe2 and Fe6 respectively, when $^{13}C^{18}O$ binds at the other Fe site. The kinetic energy distribution (KED) factors in Table S2 in the Supporting Information indicate that less than 2% of the energy is accumulated in $^{13}C^{18}O$ stretch in these modes, and $^{12}C^{16}O$ stretch accounts for the rest.

As was mentioned above, models with the same CO-binding modes and with the now-favored $\mathbf{X}=C^{4-}$ as the central ligand of the FeMo-cofactor were also considered. With the same μ^2 S2B-H protonation scheme as for the $\mathbf{X}=N^{3-}$ case, the calculations gave bound $\tilde{\nu}$(CO) frequencies $>30\,cm^{-1}$ red-shifted compared with the observed FTIR values, and optimized structures qualitatively identical to those presented in Figure 4. An extra proton addition at the μ^2 S5A FeMo-cofactor sulfur places our $\mathbf{X}=C^{4-}$ model at the same charge level (-3 units) as that of the $\mathbf{X}=N^{3-}$ model, and it significantly improves the correspondence with the FTIR experiment. For the calculated Hi-3 ($^{12}C^{16}O$ and $^{13}C^{18}O$) $\tilde{\nu}$(CO) modes, the consistent negative deviation from the FTIR peaks is 6–8 cm^{-1}, whereas for the Lo-3 modes it is positive 2–3 cm^{-1} (see Table S3 in the Supporting Information).

Discussion

Studies of the interaction of CO with N_2ase have a long history dating back to at least 1941.[4a] The subject has taken on added significance with the discovery of N_2ase Fischer–Tropsch like CO reduction and condensation chemistry.[5–8] To date, nearly all the discussion about the structure and reactivity of CO intermediates has centered about two EPR-observable species, hi-CO and lo-CO.[9–10,28] However, because integration of these EPR signals usually accounts for less than 50% of the enzyme, it is obvious that a good deal (50% or more) of N_2ase–CO chemistry has not been accounted for.

To access these EPR/electron-nuclear double resonance (ENDOR)-silent species, an FTIR-monitored photolysis technique was employed in much the same way as used in myoglobin–CO studies.[29] Our initial results under high [CO] conditions indicated the presence of a previously unrecognized species that we labeled Hi-3, which was EPR-silent and so did not correlate with any of the known EPR-active species.[15] Herein, we have elucidated the spectroscopic properties, photochemistry, and likely structures of Hi-3 and its photolysis product Lo-3. As part of assessing the significance of these new EPR-silent species, an obvious question is: what fraction of our N_2ase samples is present in these forms.

We can estimate Hi-3 abundance relative to Hi-1, by assuming that 1) Hi-1 contains a single terminal CO (as well as a second either bridging and/or more reduced CO species) bound at the FeMo-cofactor; and 2) the sum of the oscillator strengths of the Hi-3 signals at $\tilde{\nu}=1938$ and 1911 cm^{-1} (from two coupled CO oscillators) corresponds to twice the strength of the Hi-1 signal at $\tilde{\nu}=1969\,cm^{-1}$ (from a single CO). From integrating the intensities of bands shown in Figure 1, the Hi-3 population is estimated as approximately 95% that of Hi-1. Although this is only an estimate, it is clear that the Hi-3 species is a major component of the reaction mixture. From the same assumptions, Hi-1 and Hi-3 signal concentrations are both significantly higher than that of Hi-2. Previous integrations of the EPR spectra of the α-H195Q MoFe protein under high [CO] conditions found 26% hi-CO, 6% hi(5)-CO, and 8% resting state enzyme.[11d] In some of our samples, the hi-CO signal approaches 50% of the total MoFe protein. Thus, if we make the further assumption that 3) the Hi-1 IR species is the same as the hi-CO EPR species,[15] then we conclude that at least a quarter and sometimes approaching half of our samples is present as Hi-3.

The combination of IR-detected photolysis experiments and DFT calculations has allowed us to propose a model for the Hi-3 species that involves two terminal *exo* CO ligands, one bound to each of the adjacent Fe2 and Fe6 sites of the FeMo-cofactor that are bridged by the protonated μ^2 S2B sulfur (Figure 4). Vibrational coupling between these two terminal CO molecules is proposed to contribute to the approximately 27 cm^{-1} frequency splitting and helps explain the approximately 3.7:1 relative intensities of the Hi-3 bands at $\tilde{\nu}=1938$ and 1911 cm^{-1}. In the present study, such coupling was confirmed by the appearance of a new band at $\tilde{\nu}=$ 1917 cm^{-1} in samples inhibited by a mixture of $^{12}C^{16}O$ and $^{13}C^{18}O$ isotopes. Our DFT model for Hi-3 lends support to this proposal. The model gave a 29 cm^{-1} splitting and relative intensities of about 3.5:1 for the coupled $\tilde{\nu}$(CO) modes, symmetric at 1938 versus asymmetric at 1909 cm^{-1}. The long-range vibrational coupling between CO molecules bound at the Fe sites approximately 2.7 Å apart can be rationalized by 1) approximate symmetry of the proposed Hi-3 structure with respect to the plane formed by the three μ^2 S sulfurs (and the central **X** ligand); and 2) electronic delocalization inherent to the iron–sulfur clusters, such as FeMo-cofactor. Notably, this vibrational coupling may have implications to Hi-3 reactivity. Although our structural model is similar to one proposed by Hoffman and co-workers to account for properties of the hi-CO EPR signal,[10,28b] we are using it instead to account for the properties of an EPR-silent species. Our prior results for the Hi-1 IR species, which we equate with the hi-CO EPR species,[15] indicate that this form has a single terminal CO with perhaps either a bridging CO or formyl ligand.

Dance has also conducted DFT calculations on CO-inhibited FeMo-cofactor with adjacent terminal CO ligands.[24] Two of his models (designated **10** and **11**) with Fe2 *exo* and Fe6 *exo* CO ligands (for the resting state $S=1/2$ cofactor, no protons added, and by using $\mathbf{X}=N^{3-}$) most closely correspond to our current Hi-3 DFT proposal and carry the same total negative charge of $3e^-$. These models, which differ only by "coordinative allosterism" in bonding with the central atom **X**, were calculated to have somewhat lower $\tilde{\nu}$(CO) frequencies of 1914/1886 and 1904/1893 cm^{-1} for **10** and **11**, respectively, than the 1938/1911 cm^{-1} pair observed in our experiments, and the intensity ratios were less than 2:1. These shifts could possibly be brought into line with our IR and DFT results by addition of one electron, and one proton at a μ^2 S sulfur. The importance of the electron and proton count for the bound $\tilde{\nu}$(CO) frequencies and other FeMo-cofactor properties is further outlined below.

For the Lo-3 photolysis product, our favored DFT-based model places a single CO ligand in the Fe2 *exo* position, implying that the net result of photolysis is displacement of the CO ligand from Fe6 (Figure 4). We cannot exclude the possibility that photolysis of CO from the Fe2 position also occurs, with subsequent relaxation to the preferred structure. The DFT model gave a calculated $\tilde{\nu}$(CO) band at 1923 cm^{-1}, which compares well with the Lo-3 FTIR signature at 1921 cm^{-1}. The calculated intensity of this band is about 2.1:1 relative to the lower-frequency Hi-3 mode, compared with the approximately 1.7:1 ratio seen in the FTIR experiment. Dance also modeled FeMo-cofactor structures with only one CO ligand.[24] Most relevant to our proposed Lo-3 structure is his model **8**, which places CO at Fe2 *endo* and gave a calculated $\tilde{\nu}$(CO) frequency of 1904 cm^{-1}. Other models with Fe2-H and/or Fe6-H hydrides in addition to a terminal CO (such as model **12**), led to vibrational coupling of the C≡O and Fe−H stretches and introduced $\tilde{\nu}$(CO) splitting that do not correspond to our Lo-3 experimental observations.

With the current DFT calculations, the FeMo-cofactor protonation scheme and the identity of the interstitial **X** (=C^{4-}/N^{3-}/O^{2-}) ligand were both found to be important for reproducing the Hi-3 and Lo-3 FTIR spectra. The interplay of these alternatives in defining the charge state of the FeMo-cofactor model was stressed earlier, for example, in connection with both Mössbauer isomer shifts[27,30] and redox-potential calculations.[27,30b,31] For our $1e^-$ reduced Hi-3 and Lo-3 FeMo-cofactor states, we found single protonation of the cofactor at the μ^2 S2B sulfur optimal for the **X**=N^{3-} alternative, whereas double protonation at μ^2 S2B and μ^2 S5A gave the best results for **X**=C^{4-}. The **X**=N^{3-} option provided very good correspondence ($\leq$2 cm^{-1} offset) to the Hi-3 and Lo-3 signatures and allowed us to interpret the minor peaks of the mixed isotope experiment (see Figure 5), whereas the
X=C^{4-} model resulted in somewhat larger frequency shifts of up to 8 cm^{-1} with respect to the FTIR data (Table S3 in the Supporting Information). However, because observed versus computed frequency deviations of up to about 1% are inherent to the present DFT setup, our calculations cannot really discern whether **X**=N^{3-} or C^{4-}. We have no reason to doubt the **X**=C^{4-} assignment that derives from other methods.[2–3]

Before discussing how or whether the Hi-3/Lo-3 couple has a role in the inhibition of N_2 and other substrate reduction or perhaps in Fischer–Tropsch like chemistry, we need to determine, in the nomenclature used by Hoffman and coworkers,[28b,32] its "electron inventory". This refers to the number of electrons delivered from the Fe protein (called n) to form the Hi-3 species, starting from the resting state called E_0. The equation $n=s+m-p$ takes into account the number of electrons transferred to substrate (s), the number delivered to the FeMo-cofactor metals (m), and the number of electrons transferred from the P cluster (p). The EPR silence of the Hi-3 species implies that n is odd, to produce an even-electron (most likely $S=0$) Hi-3 species from the $S=3/2$ EPR-active odd-electron resting state ($n=0$). The fact that Hi-3 is stable for days or longer argues against a highly reduced species with $n\geq3$, because such a species would presumably relax by H_2 evolution. Given the preference of CO for reduced metal ions, chemical intuition also argues against a more oxidized form of the FeMo-cofactor (hence, negative values for n). We are left with $n=1$, a $1e^-$ reduced FeMo-cofactor compared with the resting MoFe protein. There is no evidence for P-cluster oxidation under these conditions, thus, $p=0$. Because the bound CO has not been reduced, $s=0$. We thus get $m=n=1$ for the FeMo-cofactor metal-ion core electron count beyond the resting state.

A recent proposal suggests that the metal core of the FeMo-cofactor has only two accessible oxidation levels, the EPR-active resting state (M^N) with $m=0$ and the one-electron-reduced EPR-silent state (M^R) with $m=1$.[32] If so, then our Hi-3 species would retain the single electron on the FeMo-cofactor and be EPR-silent, whereas the lo-CO, hi-CO, and hi(5)-CO species, being more reduced than the resting state by an even number of electrons, would be EPR-active and these "extra" electrons would be forced to reside on "substrates". Thus, the lo-CO, hi-CO, and hi(5)-CO EPR signals would come from forms of N_2ase with $m=0$ and $s=2$ for a total of $n=2$. The substrate-localized electrons could reside on either a formyl species or an as yet undetected hydride species. Partially reduced substrates are of course critical intermediates for C−C coupling reactions[33] as was demonstrated previously by the formation of a range of hydrocarbons from N_2ase-catalyzed isocyanide reduction.[34]

Is the Hi-3 (or Lo-3) species relevant to N_2ase Fischer–Tropsch chemistry? Most mechanisms for Fe-catalyzed Fischer–Tropsch chemistry posit the presence of CO-derived reactants on adjacent Fe atoms,[35] and for N_2ase, intermediates with adjacent CO or $CH_xO_{0,1}$ species[7,33] have also been proposed. Evidence for multiple binding sites in N_2ase dates back 40 years or more,[4b] but it has always been difficult to separate physically distinct binding sites on the same species from those produced by different redox levels and/or protonation states of the FeMo-cofactor. The current study is the first to demonstrate simultaneous terminal CO binding to distinct and adjacent Fe sites on the FeMo-cofactor. It thus demonstrates that two CO molecules can bind to Fe atoms only about 2.7 Å apart.

Yang et al. observed that the α-H195Q/α-V70A *Av1* double mutant was much less efficient at hydrocarbon production than the α-V70A single mutant, and they and others have suggested that α-H195 functions in delivering protons for the reduction of CO.[7,36] Disruption of this proton transfer may also explain why we see a larger fraction of the Hi-3 species in the α-H195Q *Av1* compared with the wild-type enzyme.[15] Additional work is of course needed to determine whether Hi-3 represents a requisite intermediate or a side reaction resulting from a "proton bottleneck".

Finally, the Hi-3 species is only one-electron reduced from the resting state of the enzyme. Because the reduction

of two CO molecules to C_2H_4 and two H_2O requires eight electrons and eight protons, there is a good deal of chemistry required between Hi-3 and the major product observed during CO reduction. Efforts to identify and characterize those additional species are in progress.

Experimental Section

Sample preparation: Purified α-H195Q MoFe protein and Fe protein had specific activities of 2000–2800 nmol of H_2 $(\text{min mg}^{-1}\text{ protein})^{-1}$ and 2000–2300 nmol of H_2 $(\text{min mg}^{-1}\text{protein})^{-1}$, respectively. The purified component proteins were exchanged into D_2O buffer containing HEPES (25 mM pH 7.4), $MgCl_2$ (10 mM), and NaCl (250 mM). For preparation of CO-inhibited samples, low-electron-flux conditions were obtained by using a 1:4 molar ratio of Fe protein/MoFe protein. The reaction-mixture components, which consisted of ATP (2.5 mM), $MgCl_2$ (5 mM), creatine phosphate (30 mM), 25 units mL^{-1} of creatine phosphokinase in HEPES (25 mM, pH 7.4) and sodium dithionite (20 mM) were prepared in D_2O. Turnover was accomplished under 101 kPa CO. The reaction was quenched by the addition of ethylene glycol to a final concentration of 40% after 15 min. The resulting turnover product was concentrated in an Amicon microfiltration pressure concentrator by using a regenerated cellulose PLHK ultrafiltration membrane with a 100000 molecular-weight cut off under 202 kPa CO of the same composition used for the turnover reaction.

Photolysis and FTIR spectroscopy: The sample photolysis was conducted in an Oxford liquid-He flow cryostat by using a Sutter Instruments 300 W Lambda LS xenon arc lamp. Spectra were recorded at 4 cm^{-1} resolution with a Bruker V-70v FTIR spectrometer and a MCT detector. For photolysis, the lamp was shone through the side of the cryostat oriented 90° to the IR-light path. The sample was held at 45° to both beams. This allowed the use of quartz windows for the visible light. For wavelength-dependent photolysis, a set of VersaChrome® tunable band-pass filters (Semrock) with central wavelengths at 340, 380, 410, 440, 470, 510, 550, 610, 700, and 800 nm were used.

DFT calculations: The DFT calculations were performed by using the PBE functional and the LACV3P** basis set, as implemented in JAGUAR 7.7 software. For the first- and second-row elements, LACV3P** implied a 6–311G** triple-zeta basis set including polarization function. For the Fe and Mo atoms, LACV3P** uses the Los Alamos effective core potential (ECP), and the valence part is essentially of triple-zeta quality. The geometries optimized at the PBE/LACV3P** level were used for the analytic Hessian calculations, resulting in the harmonic frequencies and IR intensities discussed in the text. The analysis of the computed vibrational normal modes has been facilitated by using our in-house Q-SPECTOR Python tool, applied to model the FTIR spectra and assess the FeMo-cofactor-bound CO modes through a kinetic energy distribution (KED) approach. Further important details are given in the Supporting Information.

Acknowledgements

This work was funded by NIH GM-65440 (S.P.C.), NSF CHE-0745353 (S.P.C.), the DOE Office of Biological and Environmental Research (S.P.C.), the Alexander von Humboldt Foundation (V.P.), and UniCat Cluster of Excellence (V.P.).

[1] a) J. W. Peters, R. K. Szilagyi, *Curr. Opin. Chem. Biol.* **2006**, *10*, 101–108; b) B. M. Barney, H.-I. Lee, P. C. D. Santos, B. M. Hoffman, D. R. Dean, L. C. Seefeldt, *Dalton Trans.* **2006**, 2277–2284; c) I. Dance, *Chem. Asian J.* **2007**, *2*, 936–946; d) J. B. Howard, D. C. Rees, *Proc. Natl. Acad. Sci. USA* **2006**, *103*, 17088–17093.

[2] T. Spatzal, M. Aksoyoglu, L. Zhang, S. L. A. Andrade, E. Schleicher, S. Weber, D. C. Rees, O. Einsle, *Science* **2011**, *334*, 940.

[3] K. M. Lancaster, M. Roemelt, P. Ettenhuber, Y. L. Hu, M. W. Ribbe, F. Neese, U. Bergmann, S. DeBeer, *Science* **2011**, *334*, 974–977.

[4] a) C. J. Lind, P. W. Wilson, *J. Am. Chem. Soc.* **1941**, *63*, 3511–3514; b) J. C. Hwang, C. H. Chen, R. H. Burris, *Biochim. Biophys. Acta Bioenerg.* **1973**, *292*, 256–270; c) J. D. Tolland, R. N. F. Thorneley, *Biochemistry* **2005**, *44*, 9520–9527.

[5] a) C. C. Lee, Y. Hu, M. W. Ribbe, *Science* **2010**, *329*, 642; b) C. C. Lee, Y. L. Hu, M. W. Ribbe, *Angew. Chem.* **2011**, *123*, 5545–5547; *Angew. Chem. Int. Ed.* **2011**, *50*, 272–275.

[6] Y. Hu, C. C. Lee, M. W. Ribbe, *Science* **2011**, *333*, 753–755.

[7] Z.-Y. Yang, D. R. Dean, L. C. Seefeldt, *J. Biol. Chem.* **2011**, *286*, 19417–19421.

[8] D. L. Gerlach, N. Lehnert, *Angew. Chem.* **2011**, *123*, 8133–8135; *Angew. Chem. Int. Ed.* **2011**, *50*, 7984–7986.

[9] a) R. C. Pollock, H. I. Lee, L. M. Cameron, V. J. Derose, B. J. Hales, W. H. Orme-Johnson, B. M. Hoffman, *J. Am. Chem. Soc.* **1995**, *117*, 8686–8687; b) P. D. Christie, H. I. Lee, L. M. Cameron, B. J. Hales, W. H. Orme-Johnson, B. M. Hoffman, *J. Am. Chem. Soc.* **1996**, *118*, 8707–8709.

[10] H.-I. Lee, L. M. Cameron, B. J. Hales, B. M. Hoffman, *J. Am. Chem. Soc.* **1997**, *119*, 10121–10126.

[11] a) D. J. Lowe, R. R. Eady, R. N. F. Thorneley, *Biochem. J.* **1978**, *173*, 277–290; b) L. C. Davis, M. T. Henzl, R. H. Burris, W. H. Orme-Johnson, *Biochemistry* **1979**, *18*, 4860–4869; c) L. M. Cameron, B. J. Hales, *Biochemistry* **1998**, *37*, 9449–9456; d) M. Sørlie, J. Christiansen, B. J. Lemon, J. W. Peters, D. R. Dean, B. J. Hales, *Biochemistry* **2001**, *40*, 1540–1549.

[12] a) V. G. Moore, R. C. Tittsworth, B. J. Hales, *J. Am. Chem. Soc.* **1994**, *116*, 12101–12102; b) Z. Maskos, K. Fisher, M. Sørlie, W. E. Newton, B. J. Hales, *J. Biol. Inorg. Chem.* **2005**, *10*, 394–406.

[13] a) S. J. George, G. A. Ashby, C. W. Wharton, R. N. F. Thorneley, *J. Am. Chem. Soc.* **1997**, *119*, 6450–6451; b) R. N. F. Thorneley, G. A. Ashby, S. J. George in *Nitrogen Fixation: From Molecules to Crop Productivity* (Eds.: F. O. Pedrosa, M. Hungria, G. Yates, W. E. Newton), Kluwer, Dordrecht, **2000**, pp. 39–40; c) Z.-Y. Yang, L. C. Seefeldt, D. R. Dean, S. P. Cramer, S. J. George, *Angew. Chem.* **2011**, *123*, 286–289.

[14] C. J. Pickett, K. A. Vincent, S. K. Ibrahim, C. A. Gormal, B. E. Smith, S. P. Best, *Chem. Eur. J.* **2003**, *9*, 76–87.

[15] L. Yan, C. H. Dapper, S. J. George, H.-X. Wang, D. Mitra, W.-B. Dong, W. E. Newton, S. P. Cramer, *Eur. J. Inorg. Chem.* **2011**, 2064–2074.

[16] A. Ansari, J. Berendzen, D. Braunstein, B. R. Cowen, H. Frauenfelder, M. K. Hong, I. E. T. Iben, J. B. Johnson, P. Ormos, T. B. Sauke, R. Scholl, A. Schulte, P. J. Steinbach, J. Vittitow, R. D. Young, *Biophys. Chem.* **1987**, *26*, 337–355.

[17] V. Pelmenschikov, W. K. Myers, W. Dong, A. Scott, L. Yan, C. H. Dapper, D. Britt, W. E. Newton, S. P. Cramer, **2012**, unpublished results.

[18] K. A. Bagley, C. J. Vangarderen, M. Chen, E. C. Duin, S. P. J. Albracht, W. H. Woodruff, *Biochemistry* **1994**, *33*, 9229–9236.

[19] R. H. Austin, K. W. Beeson, L. Eisenstein, H. Frauenfelder, I. C. Gunsalus, *Biochemistry* **1975**, *14*, 5355–5373.

[20] D. J. Darensbourg, *Inorg. Chem.* **1972**, *11*, 1606–1609.

[21] Z. Maskos, B. J. Hales, *J. Inorg. Biochem.* **2003**, *93*, 11–17.

[22] R. Sarma, B. M. Barney, S. Keable, D. R. Dean, L. C. Seefeldt, J. W. Peters, *J. Inorg. Biochem.* **2010**, *104*, 385–389.

[23] O. Einsle, F. A. Tezcan, S. L. A. Andrade, B. Schmid, M. Yoshida, J. B. Howard, D. C. Rees, *Science* **2002**, *297*, 1696–1700.

[24] I. Dance, *Dalton Trans.* **2011**, *40*, 6480–6489.

[25] M. C. Durrant, *Biochemistry* **2004**, *43*, 6030–6042.

[26] a) Y. Xiao, K. Fisher, M. C. Smith, W. Newton, D. A. Case, S. J. George, H. Wang, W. Sturhahn, E. E. Alp, J. Zhao, Y. Yoda, S. P. Cramer, *J. Am. Chem. Soc.* **2006**, *128*, 7608–7612; b) D. Lukoyanov, V. Pelmenschikov, N. Maeser, M. Laryukhin, T. C. Yang, L. Noodleman, D. R. Dean, D. A. Case, L. C. Seefeldt, B. M. Hoffman, *Inorg.*

Chem. **2007**, *46*, 11437–11449; c) V. Pelmenschikov, D. A. Case, L. Noodleman, *Inorg. Chem.* **2008**, *47*, 6162–6172.
[27] T. V. Harris, R. K. Szilagyi, *Inorg. Chem.* **2011**, *50*, 4811–4824.
[28] a) H.-I. Lee, B. J. Hales, B. M. Hoffman, *J. Am. Chem. Soc.* **1997**, *119*, 11395–11400; b) H. I. Lee, M. Sørlie, J. Christiansen, T. C. Yang, J. L. Shao, D. R. Dean, B. J. Hales, B. M. Hoffman, *J. Am. Chem. Soc.* **2005**, *127*, 15880–15890.
[29] J. O. Alben, D. Beece, S. F. Bowne, W. Doster, L. Eisenstein, H. Frauenfelder, D. Good, J. D. McDonald, M. C. Marden, P. P. Moh, L. Reinisch, A. H. Reynolds, E. Shyamsunder, K. T. Yue, *Proc. Natl. Acad. Sci. USA* **1982**, *79*, 3744–3748.
[30] a) V. V. Vrajmasu, E. L. Bominaar, E. Münck, *Inorg. Chem.* **2003**, *42*, 5974–5988; b) T. Lovell, T. Liu, D. A. Case, L. Noodleman, *J. Am. Chem. Soc.* **2003**, *125*, 8377–8383.
[31] I. Dance, *Inorg. Chem.* **2006**, *45*, 5084–5091.
[32] P. E. Doan, J. Telser, B. M. Barney, R. Y. Igarashi, D. R. Dean, L. C. Seefeldt, B. M. Hoffman, *J. Am. Chem. Soc.* **2011**, *133*, 17329–17340.
[33] I. Dance, *Dalton Trans.* **2011**, *40*, 5516–5527.
[34] M. Kelly, *Biochem. J.* **1968**, *107*, 1–6.
[35] E. de Smit, B. M. Weckhuysen, *Chem. Soc. Rev.* **2008**, *37*, 2758–2781.
[36] K. Fisher, M. J. Dilworth, W. E. Newton, *Biochemistry* **2000**, *39*, 15570–15577.

Received: June 12, 2012
Revised: August 22, 2012
Published online: November 7, 2012

